Positions of the cytoplasmic end of BK α S0 helix relative to S1–S6 and of β1 TM1 and TM2 relative to S0–S6

Guoxia Liu,[1,2]* Sergey I. Zakharov,[1,2]* Yongneng Yao,[3,4,5] Steven O. Marx,[1,2] and Arthur Karlin[3,4,5]

[1]Department of Medicine, Division of Cardiology; [2]Department of Pharmacology; and [3]Department of Biochemistry, [4]Department of Physiology, and [5]Department of Neurology, Center for Molecular Recognition, College of Physicians and Surgeons, Columbia University, New York, NY 10032

The large-conductance, voltage- and Ca^{2+}-gated K^+ (BK) channel consists of four α subunits, which form a voltage- and Ca^{2+}-gated channel, and up to four modulatory β subunits. The β1 subunit is expressed in smooth muscle, where it slows BK channel kinetics and shifts the conductance–voltage (G-V) curve to the left at $[Ca^{2+}] > 2$ μM. In addition to the six transmembrane (TM) helices, S1–S6, conserved in all voltage-dependent K^+ channels, BK α has a unique seventh TM helix, S0, which may contribute to the unusual rightward shift in the G-V curve of BK α in the absence of β1 and to a leftward shift in its presence. Such a role is supported by the close proximity of S0 to S3 and S4 in the voltage-sensing domain. Furthermore, on the extracellular side of the membrane, one of the two TM helices of β1, TM2, is adjacent to S0. We have now analyzed induced disulfide bond formation between substituted Cys residues on the cytoplasmic side of the membrane. There, in contrast, S0 is closest to the S2–S3 loop, from which position it is displaced on the addition of β1. The cytoplasmic ends of β1 TM1 and TM2 are adjacent and are located between the S2–S3 loop of one α subunit and S1 of a neighboring α subunit and are not adjacent to S0; i.e., S0 and TM2 have different trajectories through the membrane. In the absence of β1, 70% of disulfide bonding of W43C (S0) and L175C (S2–S3) has no effect on V_{50} for activation, implying that the cytoplasmic end of S0 and the S2–S3 loop move in concert, if at all, during activation. Otherwise, linking them together in one state would obstruct the transition to the other state, which would certainly change V_{50}.

INTRODUCTION

Large-conductance, voltage- and Ca^{2+}-gated K^+ (BK) channels are negative-feedback regulators of excitability in many cell types. They are complexes of four pore-forming α subunits and up to four β subunits (Butler et al., 1993; Knaus et al., 1994). The α subunit contains the S1 through S6 transmembrane (TM) helices conserved in all voltage-gated K^+ channels. In addition, BK α also has a unique seventh TM helix, S0, N-terminal to S1–S6 (Wallner et al., 1996). After S6, the ∼800 C-terminal residues contain two regulator of K^+ conductance (RCK) domains functioning as Ca^{2+} sensors (Schreiber and Salkoff, 1997; Shi et al., 2002; Xia et al., 2002; Wu et al., 2010; Yuan et al., 2010, 2012; Zhang et al., 2010). Previously, from the extent of endogenous disulfide cross-linking of Cys substituted in the predicted extracellular flanks and in the first turns in the membrane of S0 and S1–S4, we inferred that S0 is adjacent to S3 and S4 and not to S1 and S2 (Liu et al., 2008a, 2010). Compared with other V-gated K^+ channels, the V_{50} for gating charge movement of the voltage-sensor domain (VSD) of BK composed of α subunits alone is shifted to much more positive voltages. Given the proximity of the extracellular end of S0 to S3 and S4, it is possible that S0 contributes to this unusual stabilization of the deactivated state of the BK channel. We have now determined where, relative to S1–S6, S0 emerges on the intracellular side of the membrane. Our structural interpretation of a large number of cross-linking results depends on our model of BK S1–S6 (Liu et al., 2010), based on the solved structure of the homologous Kv1.2/2.1 chimera (Long et al., 2007), and on a simple optimization algorithm (described below).

There are four tissue-specific, homologous BK β subunits: β1, β2, β3, and β4 (Knaus et al., 1994; Wallner et al., 1999; Brenner et al., 2000; Uebele et al., 2000; Lu et al., 2006). The β types modulate channel function with overlapping but different repertoires. The different β subunits are 191–235 residues long, have two TM helices, TM1 and TM2, cytoplasmic N-terminal and C-terminal tails, and an extracellular loop of ∼120 residues. From disulfide cross-linking of a large number of pairs of

*G. Liu and S.I. Zakharov contributed equally to this paper. Correspondence to Steven Marx: sm460@columbia.edu; or Arthur Karlin: ak12@columbia.edu

Abbreviations used in this paper: BK, large-conductance, voltage- and Ca^{2+}-gated K^+; HRV, human rhinovirus; QPD, quaternary piperazinium diamide; RCK, regulator of K^+ conductance; SH, sulfhydryls; SSD, sum of square differences; TM, transmembrane; VSD, voltage-sensor domain.

The Rockefeller University Press $30.00
J. Gen. Physiol. Vol. 145 No. 3 185–199
www.jgp.org/cgi/doi/10.1085/jgp.201411337

substituted Cys, we previously inferred the positions relative to α S0–S6 of the extracellular ends of TM1 and TM2 in β1, β2, β3a, and β4. Although for all β types TM1 and TM2 were in the gap between adjacent VSDs with TM2 close to S0 in one subunit and TM1 close to S1 and S2 in an adjacent subunit, there were subtle differences among the β's (Liu et al., 2008b; Wu et al., 2009, 2013). At their extracellular ends, TM2 contacts S0, which in turn contacts S3 and S4. It is possible that the effects of β1, β2, and β4 on the VSD are transmitted in part through these helical contacts. We have now also determined where, relative to S0–S6, β1 TM1 and TM2 emerge on the intracellular side of the membrane.

BK channels are opened by two additive inputs, a depolarizing change in membrane potential, which activates the VSDs, and an increase in $[Ca^{2+}]_{IN}$, which increases occupation of the Ca^{2+}-binding sites. These inputs are linked through propagated changes in the structure of the channel complex, a mechanism well simulated by an allosteric kinetic model (Horrigan and Aldrich, 2002). In structures solved in two or more functional states, such changes in functional and structural states involve rigid body movements of large stable domains driven by shifting interactions of relatively small domains (for recent examples see L. Chen et al., 2014, and Yelshanskaya et al., 2014). These small domains are the pistons and gears of the machine. One requirement for us to understand how BK channels (or any other input-driven, multistate protein) work is to identify both the shifting and the stable interactions. This is our motivation to identify proximities and to determine whether covalently fixing potentially interacting positions affects function. Ironically, the least problematical result to interpret is that the cross-linking of two positions has no effect on function. We previously found that in the transition between activated and deactivated states, the extracellular end of S0 and the short S3–S4 loop moved in concert, if at all (Liu et al., 2008a, 2010; Niu et al., 2013). We now report that in the absence of β1, the intracellular end of S0 moves in concert, if at all, with the short loop between S2 and S3 and, similarly, in the presence of β1, the intracellular end of TM1 moves in concert, if at all, with the S2–S3 loop.

MATERIALS AND METHODS

Constructs

In the initial background, pseudo-WT construct pWTa (Fig. 1 E) of the mouse BK α subunit (mSlo1, KCNMA1; GenBank accession no. NM_010610), an HA epitope and a linker with extra Lys, as targets for surface biotinylation, were added to the N terminus (Fig. 1, A and C); Cys14 and Cys141 (disulfide cross-linked in WT BK α; Liu et al., 2008a) were mutated to Ala; and Cys53, Cys54, and Cys56 in the S0–S1 loop were mutated to Ser. For α to β1 cross-linking, pWTb (Fig. 1 E) was constructed with the human rhinovirus (HRV)-3C protease-consensus cleavage site, LEVLFQGP, inserted with linkers after S6 (Fig. 1, A and C). For S0 to S1–S5 cross-linking, pWTc (Fig. 1 E) was constructed with two HRV protease-consensus sites: one (site 1) in the S0–S1 loop (Liu et al., 2008a, 2010) and one (site 2) after S6 (Fig. 1, A and C). Cys substitutions in the human β1 subunit (KCNMB1; GenBank accession no. NM_004137; 191 residues) were made in a pWT β1 background with Ala substitutions at Cys18 and Cys26 (Fig. 1, B and D). HisG-pWT β1-FLAG contained an N-terminal six–His-Gly tag preceding the FLAG-epitope tag and the mutation E13Q.

Cross-linking between α and β subunits

In all intracellular cross-linking, HEK293 cells were cultured and transfected as described previously (Liu et al., 2008a,b). 2 d after transfection, the cells were surface biotinylated with 1 mM sulfosuccinimidyl-6-(biotinamido) hexanoate (sulfoNHS-LC-biotin; Thermo Fisher Scientific) in Dulbecco's phosphate-buffered saline (DPBS), pH 7.4. The cells were washed with DPBS and permeabilized with 0.07% saponin. Disulfide bond formation was induced with the bis-quaternary ammonium oxidant, 4,4′-(azodicarbonyl)-bis-[1,1-dimethylpiperazinium, diiodide] (quaternary piperazinium diamide [QPD]) (Kosower et al., 1974; Liu et al., 2008a), at a final concentration of 0.4 mM reacted for 20 min. The reaction was quenched with 2 mM *N*-ethylmaleimide, which rapidly alkylated all free sulfhydryls (SH). Cells were solubilized in lysis buffer containing 1% Triton X-100, 150 mM NaCl, 50 mM Tris, 2 mM *N*-ethylmaleimide, 1 mM EDTA, and protease inhibitors.

The lysates were mixed with Ultralink Immobilized NeutrAvidin Plus beads (Thermo Fisher Scientific), washed extensively. The beads were mixed with HRV-3C protease (EMD Millipore) overnight at 4°C. Protein was eluted in 4 M urea in 2% SDS at 100°C. Half of each sample was reduced with 10 mM DTT. The unreduced and the reduced portions were electrophoresed and transferred to nitrocellulose and immunoblotted with anti-HA antibody. Additional methods were as described previously (Liu et al., 2008a,b, 2010).

In all intracellular cross-linking, there was extensive intersubunit cross-linking between native Cys in the cytoplasmic domain of α (see Results). To analyze cross-linking involving the S1–S6 region, we removed the C-terminal domain by cleaving at a specific cleavage site for HRV-3C protease inserted just after the S6 helix. For analysis of intrasubunit cross-linking, we inserted a second HRV-3C site between S0 and S1. The extent of cleavage at these sites was determined by analysis of blots of samples that were finally completely reduced with DTT. Thus, for every sample, we could determine the fraction of cleavage, which under the conditions we used, was in the range of 50–70%. We used the actual fraction cleaved for each sample as the efficiency of cleavage, called y, for that sample. We took x as the unknown extent of cross-linking, and as shown below, we could write equations in x and y to give the expected fractions of cleaved fragments of different sizes and solve these equations for x, the desired extent of cross-linking.

For α–β cross-linking, the calculation of the cross-linking extent (x) from the immunoblot is based on the following: If "65" is the integrated density of the 65-kD band (42-kD cleaved α fragment + β1), fraction(65) = "65"/(densities of all tagged bands). Similarly, fraction(42) = "42"/(densities of all tagged bands). After DTT reduction of gel samples, fraction(42R) = "42R"/(densities of all tagged bands), and fraction(130R) = "130R"/(densities of all tagged bands) (this is the fraction of uncleaved α monomer). The efficiency of cleavage of HRV-3C sites, y = "42R"/("42R" + "130R"). If x is the fraction of α cross-linked to β, then fraction(65) = x*y. Because cleavage of un–cross-linked α results in a fragment of 42 kD (Fig. 3 A), fraction(42) = (1 − x)*y. Thus, "65"/"42" = x/(1 − x); y cancels. Thus, x = "65"/("42" + "65").

Intrasubunit cross-linking between S0 and S1–S5

We constructed double-Cys mutants with one Cys in the intracellular flank of S0 and one in the intracellular flank of S1, the S2–S3 loop, or the S4–S5 loop. (By flank, we mean the first four residues just outside the membrane domain.) S6 was excluded because Cys in the S6 flank formed intersubunit disulfides (see below). The Cys substitutions were made in the pWTc background (Fig. 1 E). Cells were exposed to 0.4 mM QPD in 0.07% saponin for 20 min. Cleavage by HRV-3C was performed as described above. The extent of cross-linking (x) was calculated based on the densities in the unreduced samples of the 13-kD band ("13") and the 42-kD band ("42"), and the densities in the reduced samples of the 13-kD band ("13R"), the 42-kD band ("42R"), and the 130-kD band ("130R"). If y_1 is the fraction of HRV-3C site 1 (in the S0–S1 loop) that is cleaved, and y_2 is the fraction of HRV-3C site 2 (after S6) that is cleaved, then y_1 = "13R"/("13R" + "42R" + "130R") = fraction(13R), and $y_2*(1 - y_1)$ = "42R"/("13R" + "42R" + "130R") = fraction(42R). In the unreduced samples, fraction(13) = "13"/D, where D = "13" +"42" + "130" + ">130," and fraction(42) = "42"/D. There is only one way to get the 13-kD band: no cross-link and cleavage at HRV-3C site 1. Hence, fraction(13) = $(1 - x)*y_1$. There are three ways to get the 42-kD band: (1) a cross-link and cleavage at HRV-3C site 2 with or (2) without cleavage at site 1, and (3) no cross-link and cleavage only at site 2; hence, fraction(42) = $x*y_2 + (1 - x)*(1 - y_1)*y_2$. D can be eliminated from the two equations in x to yield x = {Q − fraction(42R)/fraction(13R)}/{Q + fraction(42R)/[(1 − fraction(13R)]}, where Q = "42"/"13."

Cross-linking between β1 TM1 and TM2

We used cleavage of β1 by GluC endoproteinase at sites between TM1 and TM2, as described previously (Liu et al., 2010; Wu et al., 2013), to distinguish fragments that were cross-linked from those that were not. HEK cells were transfected with pWT α and the β1 double mutant G12C-R182C in the background His-FLAG-pWT β1, with the additional mutation E13Q removing a cleavage site N-terminal to Glu50. The cells were permeabilized with 0.07% saponin and disulfide cross-linking between the substituted Cys induced with 0.4 mM QPD. The cells were then solubilized with 1% Triton X-100, 200 mM NaCl, 20 mM Tris, 2 mM *N*-ethylmaleimide, and 20 mM imidazole, pH 8.0, with complete protease inhibitors (Roche). The lysate was mixed for 1 h at room temperature with 50 µl of Ni^{2+} beads (GE Healthcare), and the beads were washed four times with the same buffer. Proteins were eluted and simultaneously denatured by mixing the beads with 20 mM EDTA, 0.2% SDS, and 20 mM HEPES, pH 7.0; after elution, the eluate was held at 95°C for 4 min. Half of the eluate was deglycosylated with PNGase F (New England Biolabs, Inc.) for 3 h at 37°C. To half of each sample, GluC endoproteinase (Roche) was added and mixed at 37°C for 18 h. The samples were split again. To one half, 10 mM DTT was added, and to the other half, water was added; all aliquots were held at 50°C for 20 min. Samples were electrophoresed on a 16% Tris-Tricine gel (EC66955; Invitrogen) using Tris/Tricine/SDS buffer (161-0744; Bio-Rad Laboratories), transferred to nitrocellulose, and blotted with horseradish peroxidase–conjugated anti-FLAG antibody (Sigma-Aldrich).

Calculation of the cross-linking extent is based on the following: The extent of TM1 to TM2 cross-linking is obtained from the integrated densities of the 7.7-kD band ("7.7") and of the 13-kD band ("13") in the absence of DTT, and the density of the 7.7-kD band after DTT ("7.7R"). Fraction(13) = "13"/(densities of all tagged fragments), and fraction(7.7) and for fraction(7.7R) are defined analogously. If y is the fraction of GluC sites cleaved, y = fraction(7.7R), fraction(13) = $x*y^2$, and fraction(7.7) = $(1 - x)*y$. If Q = fraction(13)/fraction(7.7) = "13"/"7.7," then $Q = x*y/(1 - x)$, or $x = Q/(y + Q)$.

Electrophysiology

Macroscopic currents were recorded from HEK293 cells in the inside-out patch-clamp configuration at 22–24°C (Liu et al., 2008a,b). For the measurement of conductance as a function of membrane potential (G-V curves), currents were activated by depolarizing steps, in 20-mV increments, from a holding potential of −120 mV, and then deactivated by repolarization to the holding potential and tail currents were measured. The pipette solution was 150 mM KCl, 1 mM $MgCl_2$, and 5 mM TES, pH 7.4, and the bath solution was 150 mM KCl, 5 mM TES, pH 7.0, 2 mM HEDTA, and 10 µM of free Ca^{2+}. The free Ca^{2+} concentration was calculated using the Maxchelator program and confirmed using a Ca^{2+} electrode (Orion). Fresh dissolved QPD was added at a concentration of 40 µM.

Structural model of BK α and β1

BK α S1–S6 was built by homology modeling based on the crystal structure of the Kv1.2/Kv2.1 chimera (Protein Data Bank accession no. 2R9R; Long et al., 2007), using the SWISS-MODEL server (Peitsch et al., 1995; Arnold et al., 2006; Kiefer et al., 2009). We used PyMOL software (Schrödinger, LLC) and *Coot* (Emsley and Cowtan, 2004) to build S0, TM1, and TM2 as ideal α helices, and manually docked them into S1–S6, avoiding steric overlap. S0 was modeled in BK composed of α subunits alone and in BK composed of α plus β1 TM1 and TM2 helices. In the first model, the positions of the extracellular and intracellular ends of S0 were constrained to approximate the positions derived from cross-linking of S0 to S1–S5. In the second model, the extracellular and intracellular ends of S0, TM1, and TM2 were similarly constrained to approximate their positions derived from cross-linking of TM1 and TM2 to S0–S5 and of S0 to S1–S5, as described below.

Online supplemental material

Fig. S1 shows the cross-linking of S6 to S6 of two α subunits and the I-V curve of R329C before QPD and after QPD in inside-out macropatch. Fig. S2 shows intrasubunit cross-linking between S0 and S1. Fig. S3 shows the effects on V_{50} of QPD and MBTA on pWTa and T109C. The online supplemental material is available at http://www.jgp.org/cgi/content/full/jgp.201411337/DC1.

RESULTS

Induction and quantification of intracellular cross-linking

Previously, we had determined the extents of disulfide bond formation between Cys substituted in the extracellular flanks of membrane-spanning helices (Liu et al., 2008a,b, 2010; Wu et al., 2009, 2013; Niu et al., 2013). These bonds were formed endogenously by protein disulfide isomerases in the endoplasmic reticulum. We now report on the extent of disulfide bond formation between Cys facing the cytoplasm, which is normally a reducing environment. Thus, it was necessary for us to expose the cytoplasmic surface of the cell membrane to an oxidizing agent. Copper-o-phenanthroline, H_2O_2, and diamide either permeate the cell membrane or produce an oxidizing product that does, and we tested these on intact cells. We also tested the normally impermeant, bis-quaternary-ammonium diamide derivative QPD (Kosower et al., 1974) in the presence of saponin, which rendered the cell membrane permeable. Of these reagents, QPD (with saponin) induced disulfide formation most efficiently.

One invariable consequence of adding intracellular oxidizing agents, even in the absence of newly added Cys, was the formation of oligomers of α. This made the analysis of specific intrasubunit cross-linking impractical. The α subunit C-terminal to the S6 helix is intracellular and contains 24 Cys. Three additional intracellular native Cys in the S0–S1 loop were mutated to Ser in pWTa and our other background constructs (Fig. 1 E). The oxidant-induced formation of dimers, trimers, and tetramers of pWT α could only be caused by intersubunit disulfide formation between some of the C-terminal domain Cys. Following Tang et al. (2004), we mutated subsets of these

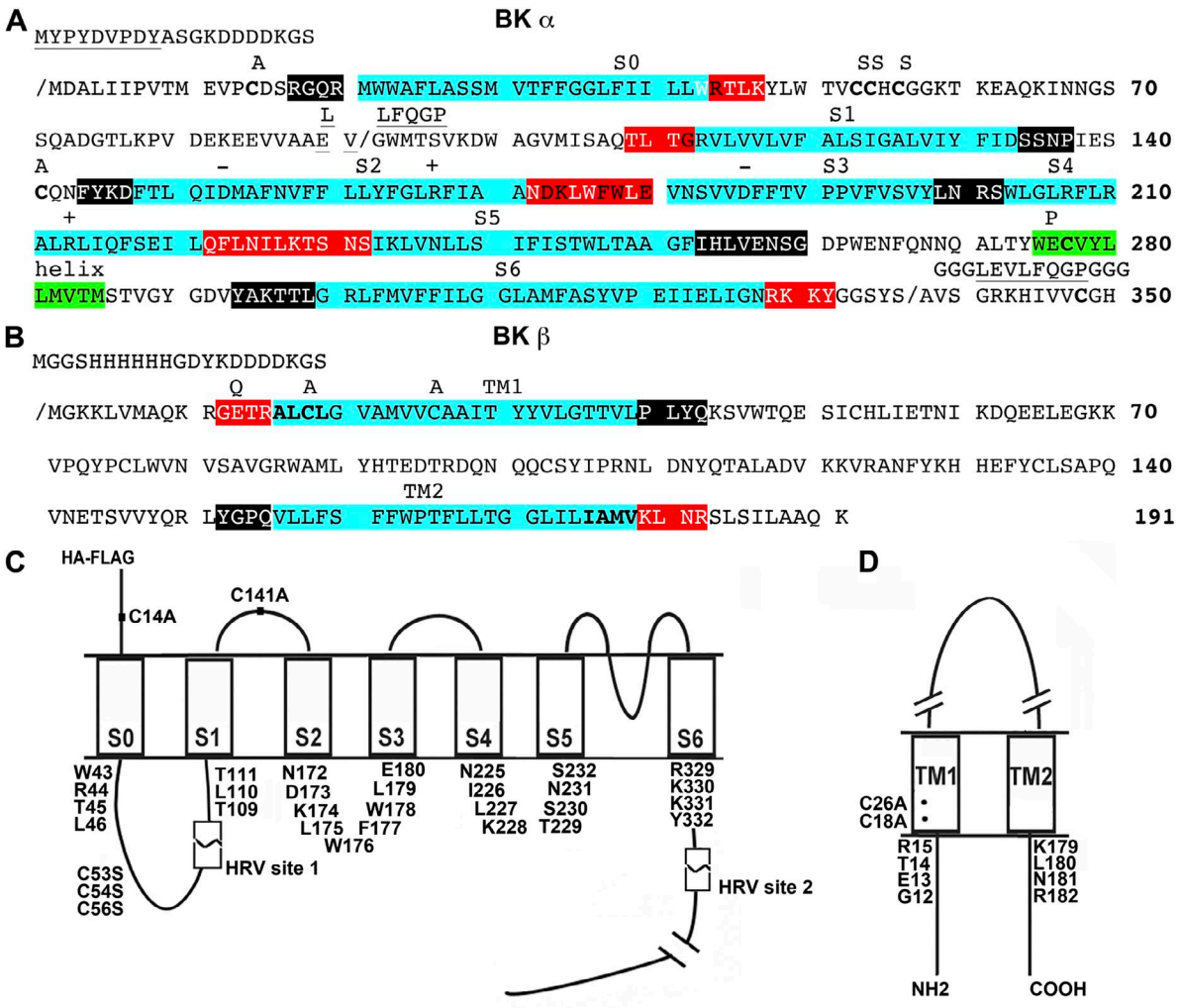

E

Construct name α	Tag	C14A, C141A (NT) (S1-S2)	C53S, C54S, C56S (S0-S1)	HRV site 1 (S0-S1)	HRV site 2 (S6-RCK1)
WT					
pWTa	X	X	X		
pWTb	X	X	X		X
pWTc	X	X	X	X	X

Figure 1. BK α and β1 subunits. (A) N-terminal 350 residues of mouse BK α (full-length 1,169 residues) with mutations and insertions above the original sequence. pWTa has an N-terminal insertion (at slash mark) of the HA epitope (underlined), followed by a linker with extra Lys as targets for surface biotinylation. Cys14 and Cys141 were mutated to Ala, and the intracellular Cys residues in the S0–S1 loop, Cys53, Cys54, and Cys56, were mutated to Ser. pWTb also has an insertion of an HRV-3C protease consensus site (underlined) with linkers after S6 (at the slash mark). pWTc has a second HRV-3C site (underlined) in the S0–S1 loop, starting at residue A89L. The extracellular residues flanking the TM helices that we previously mutated to Cys (Liu et al., 2008a) are in white letters on black; the predicted intracellular flanking residues are highlighted in red; and residues, the mutation of which to Cys yielded functional channels, are in white, and those that yielded nonfunctional channels are in black. (B) Sequence of mouse β1 with insertions and mutations in the background construct. pWT β1, in which Cys18 and Cys26 are mutated to Ala. FLAG-HIS-pWT β1 has FLAG and HIS epitopes and linker at the N terminus of pWTβ1, and the mutation E13Q. TM1 and TM2 are highlighted in cyan. The extracellular flanking residues mutated to Cys are in white letters on a black background (Liu et al., 2008b); the intracellular flanking residues mutated to Cys are in white on a red background. (C) Membrane topology of BK α showing the residues in the predicted intracellular flanks of the TM helices. The HRV-3C protease cleavage sites are shown. (D) Membrane topology of BK β1 showing residues mutated to Cys in the intracellular flanks of the TM helices. Cys18 and Cys26 within TM1 were mutated to Ala. (E) Table of α background constructs.

24 Cys to Ala, but among the mutated α's that still expressed as functional channels, the formation of oligomers persisted. We mitigated this problem by inserting an HRV-3C endoprotease cleavage site just C-terminal to S6 and N-terminal to the first native Cys (pWTb; Fig. 1, A, C, and E). After reaction with an oxidant and before SDS-PAGE, we cleaved α at this site, freeing S0–S6 from the cross-linked C-terminal domain.

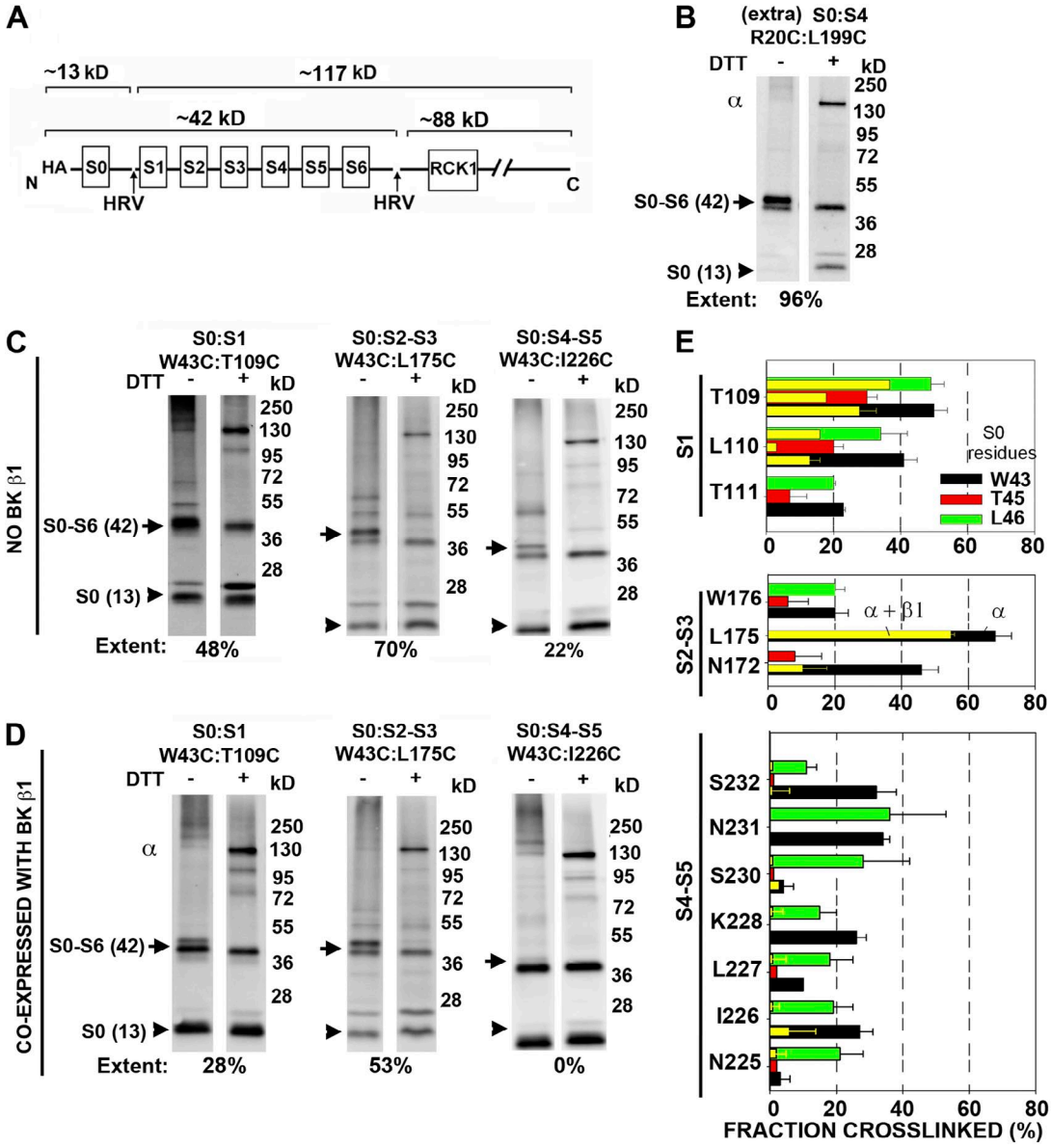

Figure 2. Intracellular cross-linking of BK α S0 to S1–S5 in the absence and the presence of β1. Expression, surface biotinylation, protein extraction, SDS-PAGE, Western blotting, and detection with an anti-HA antibody were as described previously (Liu et al., 2008a,b, 2010; Wu et al., 2009, 2013). The conditions of induction of disulfide bond formation with QPD are described in Materials and methods. (A) HRV-3C cleavage pattern. Only fragments containing the N-terminal HA epitope were detected. (B–D) Anti-HA immunoblots showing QPD-induced cross-linking between indicated Cys in S0 and S1–S5 in the absence (B and C) and presence (D) of pWT β1. (B) A highly cross-linked extracellular pair of Cys served as a positive control for the capture, cleavage, and detection of BK α. The calculated extents of cross-linking in the examples are given below the blots. (E) Mean extents (±SEM) of QPD-induced cross-linking. The wide bars are the means in the absence of β1 and are color-coded for the three residues in the intracellular flank of S0 substituted with Cys. The superimposed narrow yellow bars are the extents of cross-linking in the presence of β1. Where the extent of cross-linking is 2% or less, it is represented as 2% for visibility.

To analyze intrasubunit cross-linking between the S0 flank and S1–S6, we added another HRV-3C endoprotease cleavage site in the S0–S1 loop generating pWTc (Fig. 1 E). We called the site in the S0–S1 loop "site 1," and the one C-terminal to S6 "site 2." The pWT constructs have molecular weights of ∼130,000. The N-terminal, tagged fragment generated by cleavage at site 1 (with or without cleavage at site 2) has a molecular weight of 13,000, and the fragment generated by cleavage only at site 2 has a molecular weight of 42,000 (Fig. 2, A and B).

In α with a disulfide between a Cys in S0 and a Cys in S1–S6, cleavage at just site 2 or at both sites 1 and 2 results in a band of ∼42 kD. Both cross-linking and cleavage were incomplete. Thus, three species were generated with the same mass, 42 kD: α cross-linked and cleaved at both sites 1 and 2, α cross-linked and cleaved only at site 2, and α not cross-linked and cleaved only at site 2. Only the first of these is reduced by DTT to an N-terminal, epitope-tagged 13-kD fragment and a non–epitope-tagged 29-kD fragment. Before reduction, these species electrophoresed with slightly different mobilities. The bands overlapped and were not separately quantifiable. We used the combined density of these ∼42-kD bands and the density of the 13-D band in the samples before reduction and the densities of the 13-, 42-, and 130-kD bands in the samples after reduction to calculate the extents of cleavage and of cross-linking (see Materials and methods).

As a positive control for our analysis of intracellular cross-linking, we applied it to the cross-linking of two extracellular Cys, R20C in the flank of S0 and L199C in the S3–S4 loop, in the pWTc α background (Fig. 1 E). We found previously that in a simpler pWT background without cleavage sites, these Cys were cross-linked endogenously to the extent of 96% (Liu et al., 2008a). Using the current cleavage and quantification procedures, we obtained the same extent of cross-linking, 96% (Fig. 2 B).

Optimizing conditions of intracellular cross-linking

Induction of a disulfide with agents like QPD proceeds in two steps: (1) QPD forms an adduct with the first Cys SH, and (2) the second Cys SH displaces QPD from the first to form a disulfide. QPD also can react directly with the second Cys SH, forming an adduct before this Cys SH displaces QPD from the Cys. This side-reaction

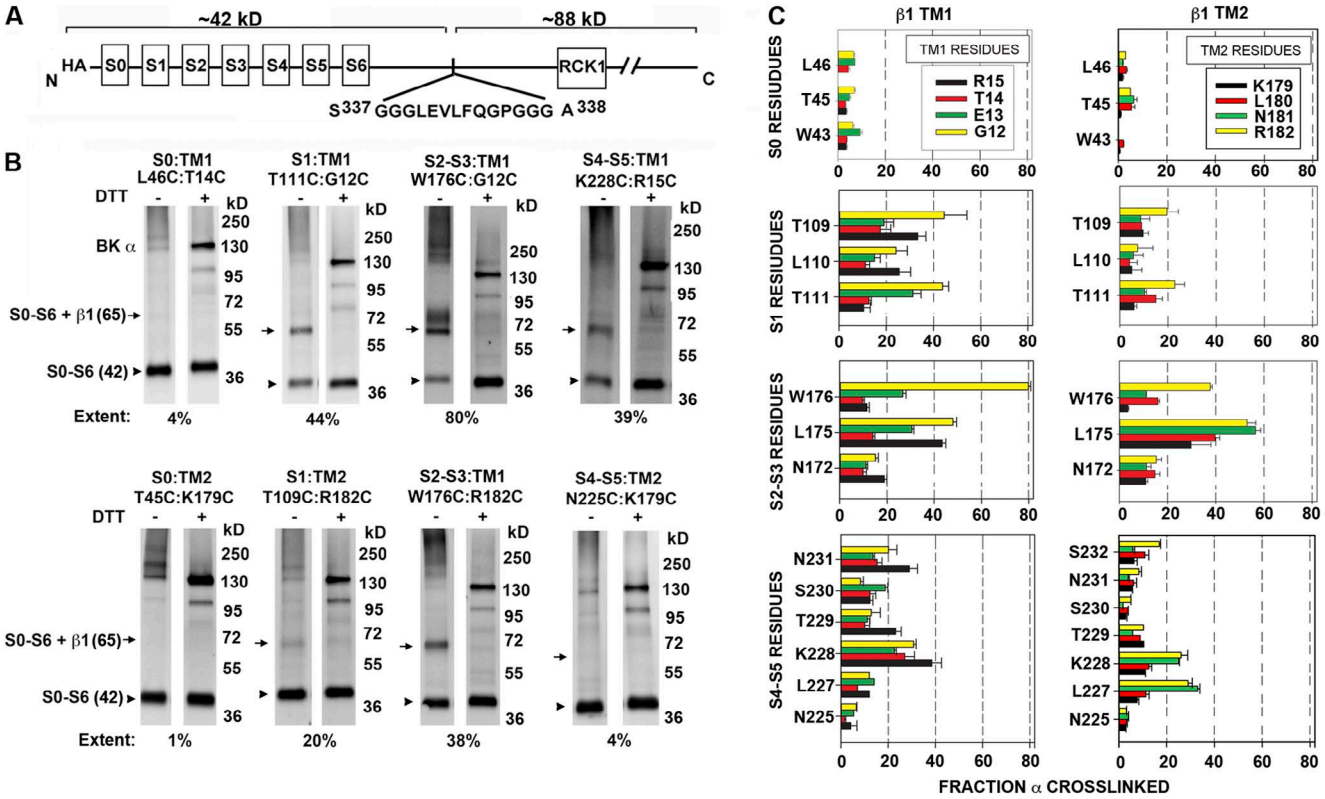

Figure 3. β1 TM1 and TM2 cross-linking to α S0–S5. (A) Cleavage at HRV-3C site 2 removed the ∼88-kD C-terminal domain. (B) Cross-linking of α and β1 and cleavage at the HRV-3C site resulted in an HA-tagged fragment of ∼65 kD (42 kD + β1). (C) Cross-linking extents between TM1 positions (left legend) or TM2 positions (right legend) and positions in S0, S1, S2–S3, and S4–S5 (vertical axes). Calculation of cross-linking extents is described in Materials and methods. Mean ± SEM.

prevents complete disulfide bond formation. The solution of the three relevant simultaneous differential equations yields:

$$x(c,t) = \{k_3/[(k_2 - 2k_1)c + k_3]\}\ \{[1 - e^{-2k_1 ct}] - [2k_1c/(k_2c + k_3)][1 - e^{-(k_2 c + k_3)t}]\},$$

where $x(c,t)$ is the fraction of the target Cys cross-linked and c is the cross-linker concentration; t is time; k_1 and k_2 are the second-order rate constants for the reactions of the cross-linker with the first and second Cys, respectively; and k_3 is the first-order rate constant for the formation of the disulfide. For any fixed time of reaction, $x(c,t)$ increases with c to a maximum and then decreases as increasingly the second Cys also forms an adduct. It is the rate constant for the formation of the disulfide, k_3, that reflects the proximity of the two Cys. Our measurement of the extent of cross-linking, however, was not precise enough to yield data that could be fit by such a kinetic equation; rather, we used the extent of cross-linking at a fixed time and QPD concentration to infer relative proximity. Taking into account the above analysis of the kinetics, however, we did determine the optimal cross-linking conditions over the concentration range of 0.1 to 0.8 mM QPD and at reaction times from 10 to 30 min. With the Cys pair, α T111C and β1 G12C, 0.4 mM QPD and a 20-min reaction time were optimal. There was no increase in the extent of cross-linking after longer reaction times. We used these conditions on all Cys pairs.

Intersubunit cross-linking of S6

Intersubunit cross-linking is a possibility that would complicate the analysis of intrasubunit cross-linking. If S0 of one subunit cross-linked to S1–S6 of a neighboring subunit, cleavage at site 1 (with or without cleavage at site 2) in the first subunit combined with cleavage just at site 2 in the second subunit would yield an ∼55-kD fragment. Cleavage of both the first subunit and the second subunit only at site 2 would yield an ∼84-kD fragment. These fragments appeared only in those double-Cys mutants in which one Cys was in the flank of S6. We tested this further in single-Cys mutants in the S6 flank in the pWTb background. In this case, cleavage at site 2 in both α's of a cross-linked dimer would yield an ∼84-kD fragment. Single-Cys mutants at each of the four positions, 329–332, in the flank of S6 were induced by QPD to form intersubunit dimers to the extent of 30–45% (Fig. S1, A and B). Functional consequences of the reaction with QPD were monitored in inside-out patches of HEK293 cells expressing αR329C; the addition of QPD caused persistent BK-conducted current even at −100 mV and a substantial leftward shift in the G-V (Fig. S1 C). The mean extent of R329C cross-linking of 45% implies that in the BK tetrameric complex, an average of approximately two of four S6 flanks were cross-linked. We do not know whether the Cys in the other two S6 flanks were derivatized by QPD without forming a disulfide. Thus, we do not know whether it is the cross-linking of S6, the addition of QPD, or both that promotes the open state. Because S6 forms intersubunit cross-links, we could not reliably determine its extent of S0–S6 intrasubunit cross-linking or its extent of α–β1 intersubunit cross-linking.

Intrasubunit cross-linking of S0 to S1–S5 in the absence and presence of β1

We determined disulfide formation between Cys substituted in the S0 intracellular flank and Cys substituted in the flanks and loops of S1–S5 (Fig. 1 C). Only mutants that were functional, defined as the presence of voltage and Ca^{2+}-dependent currents, were analyzed for cross-linking (Fig. 1, A and C).

Cys in the S0 flank formed disulfides with Cys in each of the other flanks or loops (Fig. 2, C–E). The highest extent of cross-linking was between S0 and S2–S3 (e.g., W43C to L175C, 68 ± 5%). In many cases, W43C, predicted to be closest to the membrane in the S0 flank, cross-linked to a greater extent than T45C and L46C, which are further from the membrane and might have a greater range of motion. In the S2–S3 loop, L175C is further from the predicted emergence from the membrane of S2 and S3 than other tested positions and did cross-link to the greatest extent. There were substantially greater extents of cross-linking to the S5 end of the loop than to the S4 end and the middle. In cross-linking of the S0 flank to all other segments, W43C and L46C cross-linked to greater extents than T45C, which is consistent with the first two being on the same side of a helix pointing toward S1–S5 and T45C pointing away.

We coexpressed pWT β1 with the double-Cys α mutants with the highest extents of cross-linking. In all α mutants tested, β1 decreased the extent of cross-linking (Fig. 2 E, yellow bars). This effect was most marked with S0 cross-linking to S4–S5, where the extent of cross-linking was reduced nearly to zero.

To confirm that Cys in S0 formed disulfides with Cys in S1 of the same α rather than neighboring α subunits (intersubunit cross-linking), we introduced the pairs of Cys with the highest extent of cross-linking in a background containing HRV site 2 but not HRV site 1. In the absence of DTT, cleavage at site 2 would yield an ∼84-kD fragment if and only if intersubunit cross-linking occurred. No ∼84-kD fragment was present (Fig. S2 A). In a second test for intersubunit cross-linking, we coexpressed a double-Cys–substituted mutant, W43C-T109C, in the background of pWTc, with both HRV sites, and a pWTa construct without an HA-tag. These were coexpressed at different mole ratios. If intersubunit cross-linking occurred between S0 and S1, the extent of cross-linking of HA-tagged α would have substantially decreased as the ratio of pWTa to Cys-substituted mutant

increased. This was not observed (Fig. S2 B). Thus, the cross-linking between Cys in S0 and Cys in S1 is within the same subunit.

Cross-linking α and β1 subunits

Single Cys were substituted in the intracellular flanks of S0–S5 in the pWTb background (Fig. 3 A) and in the intracellular flanks of TM1 and TM2 in the background of pWT β1 (Fig. 1 D). Among the substituted Cys in the TM1 flank, G12C, the tested Cys furthest from the membrane, cross-linked to the greatest extent to the S1 flank and to the S2–S3 loop, except that R15C, the tested Cys closest to the membrane, cross-linked at least as well as G12C to S4–S5 (Fig. 3 C). The highest extent of cross-linking overall was 80% between β1 TM1 G12C and S2–S3 W176C. In the TM2 flank, R182C, the tested Cys furthest from the membrane, and N181C, one residue closer to the membrane, cross-linked substantially more readily than K179C and L180C. Like TM1, the TM2 flank cross-linked most readily to S2–S3.

Cross-linking β1 TM1 and TM2

Based on cross-linking, we previously inferred that the extracellular ends of β1 TM1 and TM2 are close (Liu et al., 2010). The intracellular ends are at least close enough for G12C in the TM1 flank and R182C in the TM2 flanks, both four residues from the membrane, to form a disulfide to the extent of 52 ± 4% (n = 3; Fig. 4). The analysis is based on cleavage of β1 with Glu-C at Glu50 and Glu143, which yields an ∼13-kD band if the two flanks are cross-linked and a 7.7-kD band if they are not (see Materials and methods). The β1 extracellular loop is *N*-glycosylated at Asn80 and Asn142. These residues should be cut out by the Glu-C cleavages. As a control for this, we found that the deglycosylating PNGase F had no effect on the mobilities of the 13- and 7.7-kD fragments (Fig. 4 B).

Functional effects of cross-links

The lengthening of the sequence between S6 and RCK1 by the insertion of the HRV-3C protease site reduces P_o (not depicted), as predicted by the studies of Niu et al. (2004). Therefore, for functional studies, we examined the function of all single mutants and a select group of double-Cys mutants in the pWTa background, which lacks the HRV-3C sites (Fig. 1 E). We determined the functions of 17 single-Cys mutants of the intracellular flanks of S0, S1, S2–S3, S4–S5, and S6 that functioned. The V_{50}s of 12 mutants were significantly increased; the V_{50}s of two, T109C and L110C, were significantly decreased (Fig. 5 A).

The two double mutants with the highest extents of cross-linking were L46C-T109C and W43C-L175C. For these double-Cys mutants and for the single-Cys mutants of the four individual residues, we compared the V_{50}s of the mutations themselves with the V_{50}s after QPD (Fig. 5, B–I). QPD had no effect on the V_{50} of pWTa (Fig. S3 A). We know from the intersubunit cross-linking of pWT α C-terminal domain that QPD does react with native C-terminal Cys, but these reactions do not affect the V_{50} for activation. The V_{50} of L46C was barely different than the V_{50} of pWTa, and QPD had only a small effect on L46C (Fig. 5, B–E). In contrast, the V_{50} of T109C was ∼60 mV more negative than pWTa, and QPD shifted the V_{50} positively by ∼80 mV. The reaction of T109C with a quaternary ammonium maleimide

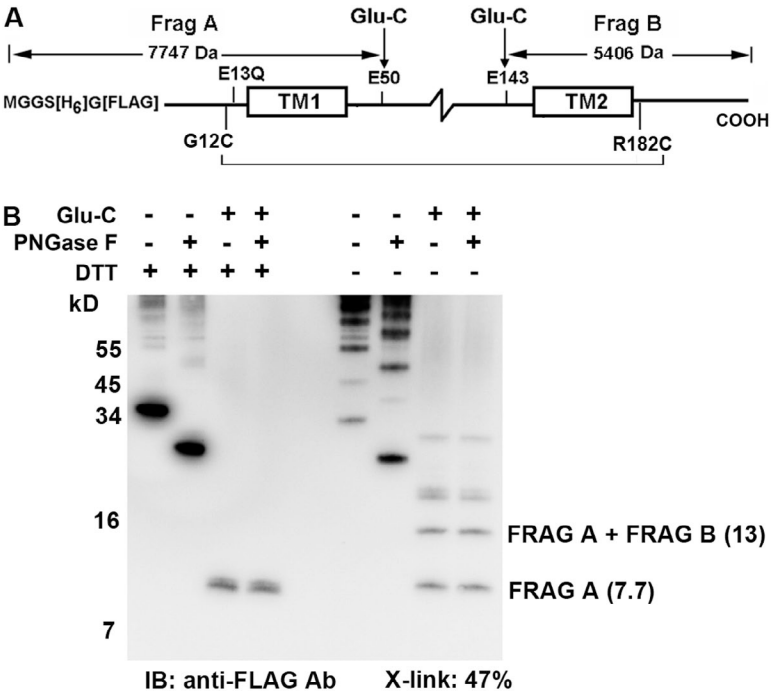

Figure 4. Cross-linking TM1 to TM2. (A) Schematic of engineered β1. Mutations G12C and R182C were made in a background of HIS-FLAG-pWT β1 with the additional mutation E13Q. In this construct, the first site susceptible to cleavage by GluC endoproteinase is C-terminal to TM1 at E50. Also, the native E143, just N-terminal to TM2, is the last E in the sequence. There are five native E's between E50 and E143, but they do not affect the outcome; complete cleavage by GluC results in an N-terminal 7,747-D fragment containing TM1 and a C-terminal 5,406-D fragment containing TM2. Their cross-linking results in a 13,153-D fragment. (B) Immunoblot with anti-FLAG antibody of β1 G12C-R182C after cross-linking with 400 µM QPD in 0.01% saponin and cleavage with GluC (see Materials and methods). Capture and immunoblotting methods were similar to those published previously (Liu et al., 2010; Wu et al., 2013). Cleavage with GluC after cross-linking yielded both an ∼13-kD band and an ∼7.7-kD band. The extent of cross-linking is calculated as (density 13-kD band)/(density 13-kD band + density 7.7-kD band). After DTT reduction, only a 7.7-kD band is seen, showing that GluC cleavage was complete.

(MBTA), which cannot lead to cross-linking, has the same effect on V_{50} as the reaction with QPD, consistent with the effect of QPD being caused by the addition of its positive charge to T109C (Fig. S3, B and C). The V_{50} of the double mutant is nearly a sum of the V_{50}s of the individual mutants, and QPD acting on the double mutant is about the sum of its effects on the two individual mutants, notwithstanding that the double mutant is ~50% cross-linked; i.e., QPD has been displaced from 25% of the Cys. Under these circumstances, it is not possible to determine separately the effects of forming an adduct with QPD and the effects of forming a disulfide. The story is different with W43C-L175C: QPD has little effect on either of the two individual Cys mutants or on the double mutant. This implies that not only are W43 in the S0 flank and L175 in the S2–S3 loop neighbors, but in addition they do not need to move relative to one another during activation and deactivation. If their relative movement were intrinsic to the transition, then linking them together in one state would obstruct the transition to the other state and destabilize it, which would certainly change the V_{50}.

We characterized the eight Cys-substituted mutants in the β1 TM1 and TM2 flanks (Fig. 6). In general, the Cys mutants of β1 function like WT β1: they shift the V_{50} of the BK channel complex to the left (in 10 µM Ca) and slow activation and deactivation. Thus, these mutants are likely to be similar to WT β1 in their association with α, so that the proximities we infer from the extents of disulfide bond formation are likely to reflect the proximities of the native residues. In detail, in each β1 Cys mutant, the time constants for activation and deactivation were greater than those for pWT (Fig. 6, A and C). Also, the V_{50} for opening of each mutant was shifted negatively relative to pWT α. We characterized two pairs of α and β1 mutants with high extents of cross-linking: W176C(S2–S3)-G12C(TM1) and W176C(S2–S3)-R182C (TM2). For these double-Cys mutants and for the single-Cys mutants of the four individual residues, we compared the V_{50}s of the mutations themselves with the V_{50}s after QPD (Fig. 6, D–H). QPD had similar effects on the individual Cys mutants and on the double mutants. This implies not only that both G12 in TM1 and R182C in TM2 are neighbors of W176C in the S2–S3 loop, but also TM1 and TM2 do not move relative to S2–S3 during activation and deactivation. If they did, then linking TM1 to S2–S3 or TM2 to S2–S3 in one state would obstruct the transition to the other state and destabilize it, which would certainly change the V_{50}.

DISCUSSION

Why disulfide cross-linking

In BK channels, like in other voltage-gated K^+ channels, the VSDs undergo structural changes in response to changes in the electrostatic field in the membrane, although there are differences in detail. The gating charge in BK channels is much smaller than that in, say, Kv1.2, the residues carrying the charges are more dispersed, and the midpoint of activation is shifted far to the right. Exactly what structural change in the VSD occurs even in the better characterized Kv1.2 is not a settled question. So far, the known structures of these channels have been obtained only in detergent and in the presumed open state. The transmission of the electrostatic field–driven changes in the VSDs to the pore and its gates has been plausibly modeled in Kv1.2/2.1 and is likely to be similar in BK channels but again different in detail (Chen and Aldrich, 2011; Zhou et al.,

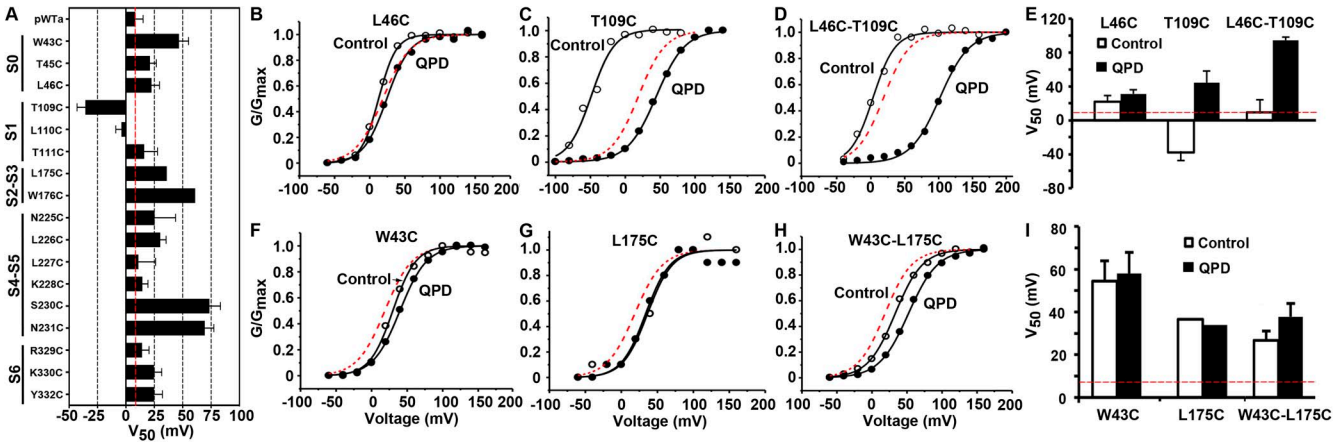

Figure 5. Effects of Cys substitutions in the intracellular flanks of S0–S6 and of their reactions with QPD on V_{50}. (A) Mean V_{50} ± SEM of the V_{50}s from the individual fits of the Boltzmann equation to the currents from each cell. n = 3–5 for each mutant. The dashed red line corresponds to mean V_{50} of pWT α. (B–D and F–H) Normalized G-V curves of untreated macropatches (control) and after treatment with 40 µM QPD for 5–7 min. The G-V curve of pWT α is shown as a dashed red line. Recordings were from inside-out macropatches with 10 µM Ca^{2+} in the bath solution. (E and I) Bar graph of V_{50}s before and after treatment with QPD for W43C, L175C, and W43C + L175C. Mean ± SEM.

2011; X. Chen et al., 2014). BK channels, similarly to MthK (Jiang et al., 2002; Yuan et al., 2010, 2012), can be activated by the binding of Ca^{2+} to intracellular RCK domains, the separate structures of which have been solved. There is evidence that the Ca^{2+}-induced structural change in the tetrameric RCK complex pulls on the cytoplasmic ends of the S6 helices (Niu et al., 2004).

What can disulfide cross-linking of substituted Cys add to these insights into the structural bases of function? Even when applied systematically, it can query only a small fraction of the possible residue-to-residue interactions in a protein. When, however, it is applied to a particular interface, as we have applied it to the interface of BK S0 with the other membrane-embedded helices of BK channels and also to the interface of BK β1 subunit TM1 and TM2 with S0–S6, it can provide new information not readily available by other means. It is well-suited to provide strong constraints on possible mechanisms involving moving parts (Yelshanskaya et al., 2014). Disulfide cross-linking also has the following advantages: the target channel is in its native environment and functional; the extent of reaction can be determined biochemically; the functional consequences of the reaction can be determined electrophysiologically; and conversely, the time course of the reaction can in favorable cases be monitored electrophysiologically while maintaining, except for brief tests of function, a fixed functional state. Furthermore, as we show here, disulfide cross-linking can be applied to the cytoplasmic surface of the membrane.

Locating the cytoplasmic ends of S0, TM1, and TM2

The susceptibility of two Cys to disulfide bond formation, which is preceded by their collision, depends in part on their proximity. It also depends on other factors that influence the collision rate and the reactivity upon collision, such as the relative orientations of the two Cys; the flexibility of the protein chain and of nearby side chains; accessibility of the Cys SH to the oxidant (in this case, QPD); and, because only the ionized thiolate has appreciable reactivity, the related factors, accessibility to water, local electrostatics, and the local pKa of the SH. The local effects on single Cys of orientation and of short-range molecular crowding could be different at neighboring positions. By testing Cys at several successive positions, we could identify the most reactive among up to 16 pairs, while still remaining within four residues of the emergence of each helix from the membrane. These Cys close to the membrane are roughly coplanar, partly justifying our use of cross-linking to locate the relative positions of two Cys in two dimensions.

Our goal was to use the extents of cross-linking to locate the cytoplasmic ends of S0, TM1, and TM2 relative

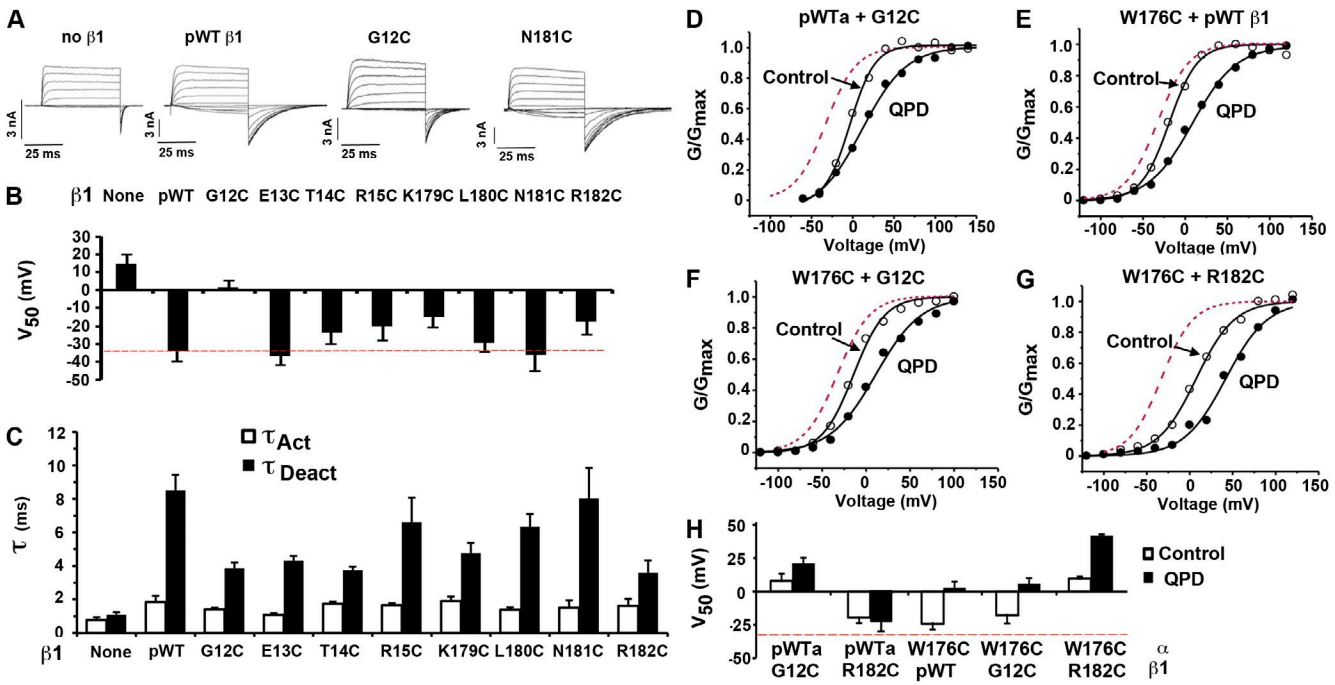

Figure 6. Functional effects of Cys substitution in the intracellular flanks of the β1 TM helices. Eight Cys-substituted mutants were expressed with pWT α in HEK 293 cells. Recordings were in inside-out macropatches with 10 μM Ca^{2+} in intracellular solution. (A) Macroscopic currents in response to step depolarizations from −100 to +140 mV conducted by pWT α coexpressed without β1 or with the indicated pWT or mutant β1. (B) V_{50} of single-Cys β1 mutants. Mean ± SEM. The mean V_{50} of pWT α + pWT β1 is shown as a dashed red line. (C) tau_{act} and tau_{deact}. Mean ± SEM; n = 3–5 for each. (D–G) Normalized G-V curves of untreated macropatches (control) and after treatment with 40 μM QPD for 5–7 min. The G-V curve of pWT α + pWT β1 is shown as a dashed red line. (H) V_{50}s before and after treatment with QPD for selected single- and double-Cys–substituted mutants. Mean ± SEM. The mean V_{50} of pWT α + pWT β1 is shown as a dashed red line.

to the cytoplasmic ends of S1–S6, as in our model (Liu et al., 2010) based on the structure of the Kv1.2/Kv2.1 chimera (Long et al., 2005a,b, 2007). This would be straightforward if the extents of cross-linking were simply inversely proportional to the distance between the target Cys. There are, however, other determinants of the extents of cross-linking, as noted above. The relative contributions of distance to the cross-linking extents, on the one hand, and of the other factors, on the other, could be different for different pairs of segments (S0 and S1, S0 and S2–S3, etc.). We made the assumption that by considering all of the segment pairs together, the location errors caused by our taking distance as the sole determinant and ignoring all other determinants would tend to cancel. We hedged this assumption, however, by taking into account segment flexibility. As explained below, we gave more weight to cross-links between Cys close to the membrane than to those further away, i.e., farther out on the flank.

Our analysis was as follows: We read the coordinates of the intracellular ends of S1–S6 from our model of BK α threaded through the structure of Kv1.2/2.1 (Long et al., 2005a,b, 2007). The model was oriented with the z axis coincident with the axis of the pore, as seen from the cytoplasmic side of the following residues, and we determined the x,y coordinates of G112(S1), N172(S2), E180(S3), Q222(S4), L227(S4–S5 loop middle), S232(S5), and R329(S6). All were close to the x,y plane, except N172 and R329, which in the model were ∼6 Å out of the plane in the extracellular direction. We took the x,y coordinates of these residues as those of the helices, as they emerged from the cytoplasmic surface of the membrane, except that L227 was taken to be the middle residue of the S4–S5 linker and otherwise treated in what follows the same as the ends of the helices. To transform the extents of cross-linking into distances between the helices as follows, we assumed that the extent of cross-linking was a linear function of the distance between the cross-linked Cys. The cross-linking extent was assumed to be zero at a distance between Cys of three helical diameters (30 Å) and 90% (<100% because of side reactions) at a distance of one helical diameter (10 Å). These assumptions determined the slope and intercept of the line. For each pair of flanks, S0 and S1, S0 and S2, S0 and S4, S0 and S4–S5-mid, and S0 and S5, we transformed cross-linking extent to distance, L_i. The calculations were performed separately with the top extents of cross-linking, the means of the top two extents of

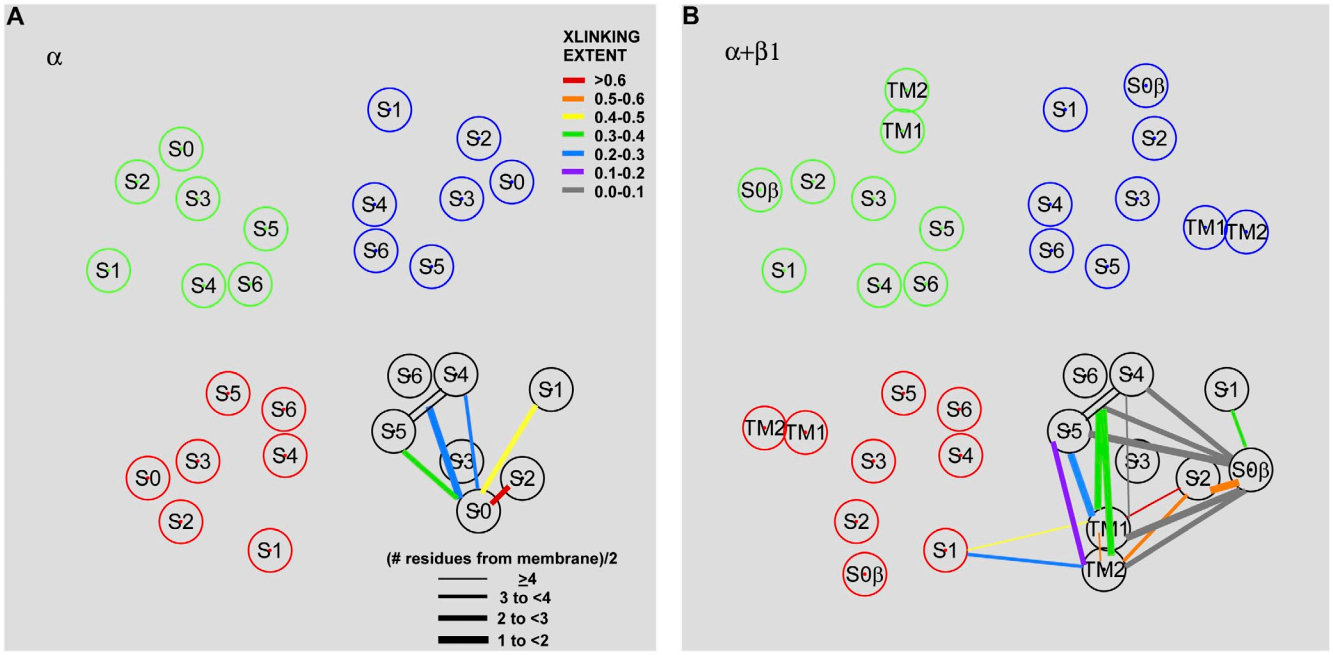

Figure 7. Optimized positions of the intracellular end of α S0, β1 TM1, and β1 TM2, relative to S1–S6 in the absence and presence of β1. The intracellular emergence of S0–S6, TM1, and TM2 from the plane of the membrane is represented as circles viewed from the cytoplasm. In one subunit of the tetramer, the top extents of disulfide cross-linking are represented as color-coded lines, the thickness of which indicates the average number of residues of the two Cys from the membrane. The inverse of these averages is used as weights for the square differences between the distances inferred from the extents of cross-linking and the distances between the unknown S0(x,y), TM1(x,y), and TM2(x,y), and the known Sn(x,y) taken from the Kv1.2/2.1 structure threaded with the BK α sequence (see Fig. 1 A). The closer the two cross-linked Cys are to the membrane, the more certainty that the extent of their cross-linking reflects the distance between the membrane-embedded helices. In an exception, the distance from S0 to the center of the S4–S5 linker (double line) is treated independently of S4 and S5. L227C at the center of the linker is taken as residue number 1, and the residues on either side of it are taken as residues 2. (A) α alone. The computation of the optimal position of S0 was based on the top extents of cross-linking. (B) The optimal position of S0 and of TM1 and TM2 was based on the top extents of cross-linking.

cross-linking, and the means of the top three top extents of cross-linking (where available). With the coordinates of S0(x,y) as unknowns, we expressed the distance of S0(x,y) to i^{th} helix, $S_i(x_i,y_i)$, with coordinates taken from the model, as $D_i = [(x - x_i)^2 + (y - y_i)^2]^{1//2}$. We formed the weighted sum of square differences (SSD),

$$SSD(x,y) = W_{S0-S1}\left(D_{S0-S1} - L_{S0-S1}\right)^2 + W_{S0-S2}\left(D_{S0-S2} - L_{S0-S2}\right)^2 + W_{S0-S4}\left(D_{S0-S4} - L_{S0-S4}\right)^2 + W_{S0-S4-S5-MID}\left(D_{S0-S4-S5-MID} - L_{S0-S4-S5-MID}\right)^2 + W_{S0-S5}\left(D_{S0-S5} - L_{S0-S5}\right)^2.$$

S0–S3 is not included because three of the four Cys mutants in the S3 flank were not functional, and S0–S6 is not included because Cys in the S6 flank formed disulfides with neighboring S6 Cys. The weights were based on the average number of residues the two Cys were away from the membrane. If, for example, one residue were the first residue in flank just emerging from the membrane and the other Cys were the third residue in the flank, then the weight would be 1/[(1 + 3)/2] = 1/2. Thus, the cross-linking of Cys close to the emergence of the helices from the membrane was given greater weight than the cross-linking of Cys further from the membrane.

The unknown x,y coordinates of S0 were obtained by minimizing SSD(x,y), subject to the constraints that S0 is further than one helical diameter (10 Å) from S1 through S6 (center-to-center). The computation was performed with the minerr function in Mathcad 15 (our program is available on request).

In the presence of β1, the cross-linking of TM1 and of TM2 to each of S0–S5 and of S0 to each of S1–S5 (S3 and S6 excluded as above) was included in the weighted SSD, $SSD(x,y,x_{TM1},y_{TM1},x_{TM2},y_{TM2})$, which in this case was a function of three pairs of unknown coordinates. The error was estimated by dividing SSD by the sum of the weights and taking the square root. The errors with and without β1 were the smallest for the results based on the top extents of cross-linking (Fig. 7). These errors were 4.4 Å for α alone and 4.5 Å for α plus β1. The program was also run with no weights. The coordinates were close to those obtained with weights but with slightly larger errors.

Every aspect of this analysis has uncertainties: the model of BK α based on Kv1.2/2.1, the identification of the exact residues at the cytoplasmic ends of S1–S6 as they emerge from the bilayer, their coordinates, the exclusion of all factors except proximity (and to some extent flexibility) in the determination of the extent of cross-linking, and the assumed linear relationship of distance to the extent of cross-linking. Also, we must assume that the arrangements of S1–S6 do not change with the addition of β1. Without such an analysis, however, it would be difficult to visualize the implications of the cross-linking data, which were more complex than those on the extracellular side of the membrane. In the present minimum-error analysis, low extents of cross-linking

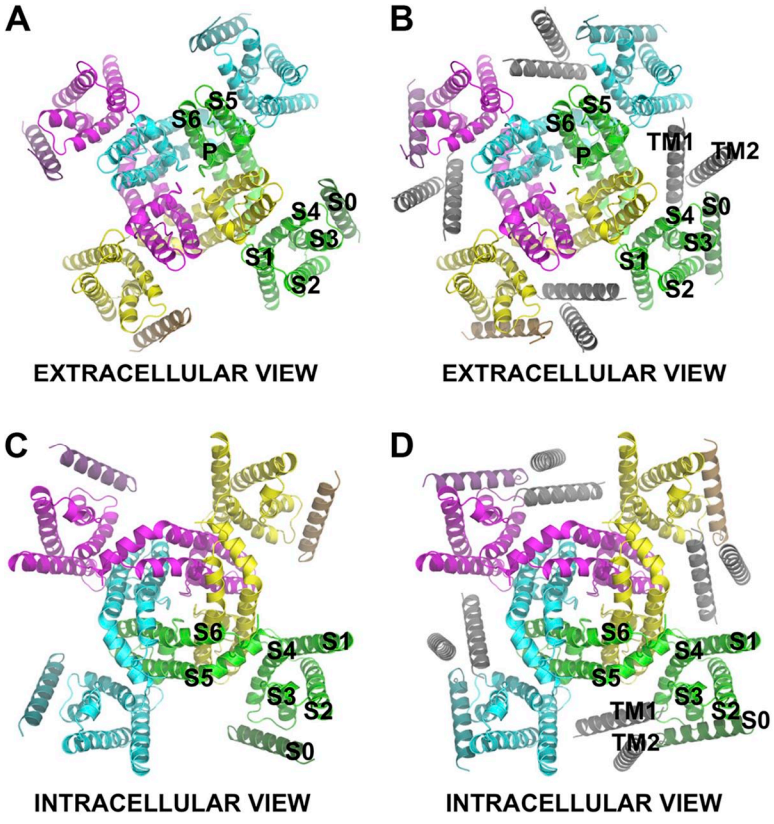

Figure 8. Model of BK α in the absence and presence of β1. BK α S1–S6 was built by homology modeling based on the crystal structure of the Kv1.2/Kv2.1 chimera (Protein Data Bank accession no. 2R9R), using the SWISS-MODEL server (Schwede et al., 2003; Arnold et al., 2006; Kiefer et al., 2009). We used PyMol and *Coot* (Emsley and Cowtan, 2004) to build S0, TM1, and TM2 as ideal α helices and manually docked them into S1–S6, avoiding steric overlap, but we did not minimize the energy of the structure. The model shows the displacement of the intracellular flank of S0 when β1 is coexpressed with α. Each subunit has a unique color. β1 TM1 and TM2 are black. (A and C) α alone. (B and D) α + β1.

had the same importance as high extents of cross-linking. The low extents fed into the algorithm were still the greatest extents among consistently low extents over many pairs in the same flanks.

Individually, some pairs of segments are more consistent with their extents of cross-linking than others. For example, in the absence of β1, S0 is too far from S1, and in the presence of β1, S0 is too close to β1 (Fig. 7). Of course, there are enough ignored other factors that could increase or decrease their extents of cross-linking.

We previously generated a space-filling model of BK-containing α subunits alone. The structures and positions of S1–S6 were based on the crystal structure of the Kv1.2/Kv2.1 chimera (Long et al., 2007), and the position of S0 was based on cross-linking between the extracellular end of S0 and the extracellular ends of S1–S6 (Liu et al., 2010). Also, we modeled BK α and β1, positioning TM1 and TM2 based on the cross-linking of their extracellular ends to S0–S6. We have now revised those models taking into account the cross-linking of the helical ends on the intracellular side of the membrane (Fig. 8). Although the new models are shown in a ribbon representation of the backbone, overlap was avoided in the full space-filling versions. In the new models, the positions of the extracellular ends of S0, TM1, and TM2 have not changed, but the positions of their intracellular ends have changed to correspond approximately to the optimized positions derived from cross-linking. S0 has not been displaced by TM1 quite as far in the space-filling model (Fig. 8) as in the optimized projection (Fig. 7). The space-filling models show that the optimized positions at the intracellular ends of the helices are compatible with the previously inferred positions at the extracellular ends of the helices, even with ideal helical configurations for S0, TM1, and TM2. What changes with the addition of β1 to the BK complex is the trajectory of S0 across the membrane.

The qualitative conclusions of the analysis are that the intracellular end of S0 is close to the S2–S3 loop in the absence of β1, that β1 causes S0 to relocate by 1 to 2 helical diameters, that TM1 takes the former position of S0 close to the S2–S3 loop, and that TM1 and TM2 emerge from the membrane together.

Implications of cross-linking for mechanisms

Previously, we determined that on the extracellular side of the membrane, S0 was juxtaposed to the short loop between S3 and S4. Surprisingly, even after 95% cross-linking of S0 to S3–S4, there was no effect on the V_{50} for BK channel opening. Thus, the extracellular end of S0 need not move relative to S3–S4. Yet, S3 and S4 make important contributions to the gating charge and must move during activation. Thus, it is likely that S3 and S4 do move and that S0 moves in concert with them. A different conclusion, based on fluorescence quenching, was that S0 separates from S3–S4 during activation (Pantazis et al., 2010). Our result implies, strictly speaking, only that they need not move apart during activation, not that they cannot move apart, even though that movement has no functional consequences. In this work, we have identified positions at the cytoplasmic end of S0 and on the short S2–S3 loop and, in the presence of β1, between the cytoplasmic end of TM1 and the S2–S3 loop, the disulfide cross-linking of which has no effect on the V_{50} for activation, again indicating that these segments need not move relative to one another during activation and deactivation. If they did need to move apart and were constrained by the 3-Å disulfide bond, one state would be destabilized relative to the other, and the V_{50} would be affected.

In the absence of β1, BK activation occurs at unusually large positive potentials. The V_{50} for activation is shifted to less positive potentials with increasing $[Ca^{2+}]_{IN}$ but not into the physiologically relevant range for smooth muscle. Only with β1 as part of the complex do V_m and Ca^{2+} act in concert in their physiological ranges, so that BK acts like a Ca^{2+} sensor around the smooth muscle resting potential. BK responds to Ca^{2+} in the micromolar range, 10 times the 100-nM range of smooth muscle cytoplasmic Ca^{2+}: this higher range is obtained in the junctional microdomains where BK faces the ryanodine receptor across a narrow gap between the sarcolemma and the sarcoplasmic reticulum. A paradox is that at $[Ca^{2+}]_{IN} < 2$ μM, β1 increases the V_{50} for activation. From our results and those of others, a rough picture emerges in which the interaction of the unique S0 with S3–S4 on the extracellular side and with S2–S3 on the intracellular side contributes to the far right shift in the G-V curve of BK consisting of α alone and that, as shown here, β1 displaces S0 on the intracellular side but not on the extracellular side (Liu et al., 2010); i.e., the path of S0 through the membrane must change with the addition of β1. Furthermore, TM1 takes the place of S0 in its interaction with the S2–S3 loop. These conclusions suggest only where the action might take place, not yet how.

This work was supported in part by National Institutes of Health research grant awards R01 NS054946 from the National Institute of Neurological Disorders and Stroke, and the Arlene and Arnold Goldstein Family Foundation.

The authors declare no competing financial interests.

Kenton J. Swartz served as editor.

Submitted: 26 November 2014
Accepted: 22 January 2015

REFERENCES

Arnold, K., L. Bordoli, J. Kopp, and T. Schwede. 2006. The SWISS-MODEL workspace: a web-based environment for protein structure homology modelling. *Bioinformatics.* 22:195–201. http://dx.doi.org/10.1093/bioinformatics/bti770

Brenner, R., T.J. Jegla, A. Wickenden, Y. Liu, and R.W. Aldrich. 2000. Cloning and functional characterization of novel large conductance calcium-activated potassium channel beta subunits,

hKCNMB3 and hKCNMB4. *J. Biol. Chem.* 275:6453–6461. http://dx.doi.org/10.1074/jbc.275.9.6453

Butler, A., S. Tsunoda, D.P. McCobb, A. Wei, and L. Salkoff. 1993. mSlo, a complex mouse gene encoding "maxi" calcium-activated potassium channels. *Science.* 261:221–224. http://dx.doi.org/10.1126/science.7687074

Chen, L., K.L. Dürr, and E. Gouaux. 2014. X-ray structures of AMPA receptor-cone snail toxin complexes illuminate activation mechanism. *Science.* 345:1021–1026. http://dx.doi.org/10.1126/science.1258409

Chen, X., and R.W. Aldrich. 2011. Charge substitution for a deep-pore residue reveals structural dynamics during BK channel gating. *J. Gen. Physiol.* 138:137–154. http://dx.doi.org/10.1085/jgp.201110632

Chen, X., J. Yan, and R.W. Aldrich. 2014. BK channel opening involves side-chain reorientation of multiple deep-pore residues. *Proc. Natl. Acad. Sci. USA.* 111:E79–E88. http://dx.doi.org/10.1073/pnas.1321697111

Emsley, P., and K. Cowtan. 2004. *Coot*: model-building tools for molecular graphics. *Acta Crystallogr. D Biol. Crystallogr.* 60:2126–2132. http://dx.doi.org/10.1107/S0907444904019158

Horrigan, F.T., and R.W. Aldrich. 2002. Coupling between voltage sensor activation, Ca^{2+} binding and channel opening in large conductance (BK) potassium channels. *J. Gen. Physiol.* 120:267–305. http://dx.doi.org/10.1085/jgp.20028605

Jiang, Y., A. Lee, J. Chen, M. Cadene, B.T. Chait, and R. MacKinnon. 2002. Crystal structure and mechanism of a calcium-gated potassium channel. *Nature.* 417:515–522. http://dx.doi.org/10.1038/417515a

Kiefer, F., K. Arnold, M. Künzli, L. Bordoli, and T. Schwede. 2009. The SWISS-MODEL Repository and associated resources. *Nucleic Acids Res.* 37:D387–D392. http://dx.doi.org/10.1093/nar/gkn750

Knaus, H.G., K. Folander, M. Garcia-Calvo, M.L. Garcia, G.J. Kaczorowski, M. Smith, and R. Swanson. 1994. Primary sequence and immunological characterization of beta-subunit of high conductance Ca^{2+}-activated K^+ channel from smooth muscle. *J. Biol. Chem.* 269: 17274–17278.

Kosower, E.M., N.S. Kosower, H. Kenety-Londner, and L. Levy. 1974. Glutathione. IX. New thiol-oxidizing agents: DIP, DIP+1, DIP+2. *Biochem. Biophys. Res. Commun.* 59:347–351. http://dx.doi.org/10.1016/S0006-291X(74)80213-5

Liu, G., S.I. Zakharov, L. Yang, S.X. Deng, D.W. Landry, A. Karlin, and S.O. Marx. 2008a. Position and role of the BK channel α subunit S0 helix inferred from disulfide crosslinking. *J. Gen. Physiol.* 131:537–548. http://dx.doi.org/10.1085/jgp.200809968

Liu, G., S.I. Zakharov, L. Yang, R.S. Wu, S.X. Deng, D.W. Landry, A. Karlin, and S.O. Marx. 2008b. Locations of the beta1 transmembrane helices in the BK potassium channel. *Proc. Natl. Acad. Sci. USA.* 105:10727–10732. http://dx.doi.org/10.1073/pnas.0805212105

Liu, G., X. Niu, R.S. Wu, N. Chudasama, Y. Yao, X. Jin, R. Weinberg, S.I. Zakharov, H. Motoike, S.O. Marx, and A. Karlin. 2010. Location of modulatory β subunits in BK potassium channels. *J. Gen. Physiol.* 135:449–459. http://dx.doi.org/10.1085/jgp.201010417

Long, S.B., E.B. Campbell, and R. Mackinnon. 2005a. Crystal structure of a mammalian voltage-dependent Shaker family K^+ channel. *Science.* 309:897–903. http://dx.doi.org/10.1126/science.1116269

Long, S.B., E.B. Campbell, and R. Mackinnon. 2005b. Voltage sensor of Kv1.2: Structural basis of electromechanical coupling. *Science.* 309:903–908. http://dx.doi.org/10.1126/science.1116270

Long, S.B., X. Tao, E.B. Campbell, and R. MacKinnon. 2007. Atomic structure of a voltage-dependent K^+ channel in a lipid membrane-like environment. *Nature.* 450:376–382. http://dx.doi.org/10.1038/nature06265

Lu, R., A. Alioua, Y. Kumar, M. Eghbali, E. Stefani, and L. Toro. 2006. MaxiK channel partners: physiological impact. *J. Physiol.* 570:65–72. http://dx.doi.org/10.1113/jphysiol.2005.098913

Niu, X., X. Qian, and K.L. Magleby. 2004. Linker-gating ring complex as passive spring and Ca^{2+}-dependent machine for a voltage- and Ca^{2+}-activated potassium channel. *Neuron.* 42:745–756. http://dx.doi.org/10.1016/j.neuron.2004.05.001

Niu, X., G. Liu, R.S. Wu, N. Chudasama, S.I. Zakharov, A. Karlin, and S.O. Marx. 2013. Orientations and proximities of the extracellular ends of transmembrane helices S0 and S4 in open and closed BK potassium channels. *PLoS ONE.* 8:e58335. http://dx.doi.org/10.1371/journal.pone.0058335

Pantazis, A., A.P. Kohanteb, and R. Olcese. 2010. Relative motion of transmembrane segments S0 and S4 during voltage sensor activation in the human BK_{Ca} channel. *J. Gen. Physiol.* 136:645–657.

Peitsch, M.C., T.N. Wells, D.R. Stampf, and J.L. Sussman. 1995. The Swiss-3DImage collection and PDB-Browser on the World-Wide Web. *Trends Biochem. Sci.* 20:82–84. http://dx.doi.org/10.1016/S0968-0004(00)88963-X

Schreiber, M., and L. Salkoff. 1997. A novel calcium-sensing domain in the BK channel. *Biophys. J.* 73:1355–1363. http://dx.doi.org/10.1016/S0006-3495(97)78168-2

Schwede, T., J. Kopp, N. Guex, and M.C. Peitsch. 2003. SWISS-MODEL: an automated protein homology-modeling server. *Nucleic Acids Res.* 31:3381–3385. http://dx.doi.org/10.1093/nar/gkg520

Shi, J., G. Krishnamoorthy, Y. Yang, L. Hu, N. Chaturvedi, D. Harilal, J. Qin, and J. Cui. 2002. Mechanism of magnesium activation of calcium-activated potassium channels. *Nature.* 418:876–880. http://dx.doi.org/10.1038/nature00941

Tang, X.D., M.L. Garcia, S.H. Heinemann, and T. Hoshi. 2004. Reactive oxygen species impair Slo1 BK channel function by altering cysteine-mediated calcium sensing. *Nat. Struct. Mol. Biol.* 11:171–178. http://dx.doi.org/10.1038/nsmb725

Uebele, V.N., A. Lagrutta, T. Wade, D.J. Figueroa, Y. Liu, E. McKenna, C.P. Austin, P.B. Bennett, and R. Swanson. 2000. Cloning and functional expression of two families of beta-subunits of the large conductance calcium-activated K^+ channel. *J. Biol. Chem.* 275: 23211–23218. http://dx.doi.org/10.1074/jbc.M910187199

Wallner, M., P. Meera, and L. Toro. 1996. Determinant for beta-subunit regulation in high-conductance voltage-activated and Ca^{2+}-sensitive K^+ channels: An additional transmembrane region at the N terminus. *Proc. Natl. Acad. Sci. USA.* 93:14922–14927. http://dx.doi.org/10.1073/pnas.93.25.14922

Wallner, M., P. Meera, and L. Toro. 1999. Molecular basis of fast inactivation in voltage and Ca^{2+}-activated K^+ channels: A transmembrane beta-subunit homolog. *Proc. Natl. Acad. Sci. USA.* 96: 4137–4142. http://dx.doi.org/10.1073/pnas.96.7.4137

Wu, R.S., N. Chudasama, S.I. Zakharov, D. Doshi, H. Motoike, G. Liu, Y. Yao, X. Niu, S.X. Deng, D.W. Landry, et al. 2009. Location of the beta 4 transmembrane helices in the BK potassium channel. *J. Neurosci.* 29:8321–8328. http://dx.doi.org/10.1523/JNEUROSCI.6191-08.2009

Wu, R.S., G. Liu, S.I. Zakharov, N. Chudasama, H. Motoike, A. Karlin, and S.O. Marx. 2013. Positions of β2 and β3 subunits in the large-conductance calcium- and voltage-activated BK potassium channel. *J. Gen. Physiol.* 141:105–117. http://dx.doi.org/10.1085/jgp.201210891

Wu, Y., Y. Yang, S. Ye, and Y. Jiang. 2010. Structure of the gating ring from the human large-conductance Ca^{2+}-gated K^+ channel. *Nature.* 466:393–397. http://dx.doi.org/10.1038/nature09252

Xia, X.M., X. Zeng, and C.J. Lingle. 2002. Multiple regulatory sites in large-conductance calcium-activated potassium channels. *Nature.* 418:880–884. http://dx.doi.org/10.1038/nature00956

Yelshanskaya, M.V., M. Li, and A.I. Sobolevsky. 2014. Structure of an agonist-bound ionotropic glutamate receptor. *Science.* 345:1070–1074. http://dx.doi.org/10.1126/science.1256508

Yuan, P., M.D. Leonetti, A.R. Pico, Y. Hsiung, and R. MacKinnon. 2010. Structure of the human BK channel Ca^{2+}-activation apparatus at 3.0 Å resolution. *Science*. 329:182–186. http://dx.doi.org/10.1126/science.1190414

Yuan, P., M.D. Leonetti, Y. Hsiung, and R. MacKinnon. 2012. Open structure of the Ca^{2+} gating ring in the high-conductance Ca^{2+}-activated K^+ channel. *Nature*. 481:94–97. http://dx.doi.org/10.1038/nature10670

Zhang, G., S.Y. Huang, J. Yang, J. Shi, X. Yang, A. Moller, X. Zou, and J. Cui. 2010. Ion sensing in the RCK1 domain of BK channels. *Proc. Natl. Acad. Sci. USA*. 107:18700–18705. http://dx.doi.org/10.1073/pnas.1010124107

Zhou, Y., X.M. Xia, and C.J. Lingle. 2011. Cysteine scanning and modification reveal major differences between BK channels and Kv channels in the inner pore region. *Proc. Natl. Acad. Sci. USA*. 108:12161–12166. http://dx.doi.org/10.1073/pnas.1104150108